Proceedings of the ASME 2010 3rd Joint US-European Fluids Engineering Summer Meeting and 8th International Conference on Nanochannels, Microchannels, and Minichannels
FEDSM-ICNMM2010
August 1-5, 2010, Montreal, Canada

FEDSM-ICNMM2010-30908

A COMPARATIVE STUDY OF INTERFACE SCHEMES IN THE IMMERSED BOUNDARY METHOD FOR A MOVING SOLID BOUNDARY PROBLEM USING THE LATTICE BOLTZMANN METHOD

Shin K. Kang
Texas A&M University
College Station, Texas, USA

Yassin A. Hassan
Texas A&M University
College Station, Texas, USA

ABSTRACT

For moving boundary problems, previous body-conformal grid methods require frequent re-meshing as the boundary moves, thus increasing computational cost. An immersed boundary method (IBM) is an attractive method to resolve the problem since it is based on the fixed, non-body-conformal grids. In the IBM, force density terms are used so that no-slip boundary condition is satisfied on the boundary. On the other hand, lattice Boltzmann methods (LBMs) have been used as an alternative of Navier-Stokes equation method due to their efficiency to parallelize and simplicity to implement. The common feature of the IBM and the LBM of using non-body-conformal grids motivated the use of the IBM in the lattice Boltzmann method frame, which is usually called an immersed boundary-lattice Boltzmann method (IB-LBM). Besides, a split-forcing property in the LBM, due to its kinetic nature, facilitates the use of direct-forcing IBM. For the evaluation of boundary force density term, we need to adopt an interpolation scheme because the boundary, in general, does not match computational nodes. The interpolation schemes can be classified into diffuse and sharp interface schemes. The former usually uses the discrete delta function to evaluate the boundary force on the prescribed boundary points, while the latter uses interpolation from neighboring fluid nodes to evaluate the boundary force on the computation node either inside or outside closest to the boundary. In the diffuse scheme, the boundary force density terms evaluated on the boundary points should be distributed onto neighboring computational nodes using the discrete delta functions so that the boundary effect may exert on computational process.

The objective of this study is to compare two interface schemes simultaneously for a moving boundary problem under the IB-LBM and to understand advantages and disadvantages of each scheme. We considered a problem of flow induced by inline oscillation of a circular cylinder since both experimental and body-conformal grid method results are available for this problem. Velocity results from both schemes showed overall good agreement with experimental data. However, the sharp interface scheme showed spurious oscillations in the surface force coefficient and pressure fields, although after filtering or smoothing, the force coefficients showed good agreement with the body-fitted results. In contrast, the diffuse interface scheme produced smooth variations in the surface force coefficient but over-predicted the absolute values especially at phase angles with the high magnitude of accelerations. These results can be attributed to the use of discrete delta functions. We could reduce the over-prediction by considering the effect of the diffuse area.

INTRODUCTION

The suitable treatment of complex, moving boundary problems is one of challenging issues in the computational fluid dynamics (CFD) field. Various methods, such as the arbitrary Lagrangian Eulerian (ALE) method (Hu et al., 2001), the Chimera method, Lagrange multiplier method (Glowinsky et al., 1999; Glowinsky et al., 2001), and the immersed boundary method (IBM), have been developed for these problems. Among the numerical methods, much attention has been paid on the IBM mainly because of its efficiency and accuracy.

The immersed boundary method (IBM) can be defined as a non-body conformal grid method, which adds a force density (or acceleration) term either explicitly or implicitly to the flow governing equation in order to satisfy the no-slip conditions on the boundary (Kang and Hassan, 2010). The use of the fixed, structured non-body-conformal grid (usually the Cartesian grid)

relieves the burden of meshing and frequent re-meshing and reduces computational cost compared to unstructured body-fitted grid and other methods, and the accurate evaluation of the force density term maintains a high accuracy.

Since Peksin (1972) pioneered the IBM, many variants of the IBM have been developed. Two key factors characterizing the IBMs are (i) the methods to evaluate the boundary force and (ii) the interface schemes to resolve the non-matching problem between boundaries and non-conformal computational nodes.

For the methods to evaluate the boundary force, the feedback forcing methods and direct-forcing methods are usually considered. In the feedback forcing method, force density term (or acceleration term) is determined by straight feedback of velocity information, i.e. time integration of the velocity difference between calculated velocity and desired velocity (production) and the velocity difference itself (damping) as follows (Goldstein et al. 1993):

$$\mathbf{F} = \alpha \int_0^t (\mathbf{u} - \mathbf{U}^d) d\tau + \beta (\mathbf{u} - \mathbf{U}^d) \quad (1)$$

where $\mathbf{U}_d$ is the desired velocity and α and β are two free parameters to be tuned depending on the flow conditions, which is a disadvantage of the feedback forcing method. Furthermore, it is known that for unsteady flows this can cause a time step limitation that reduces the efficiency. In contrast, in the direct forcing method, the force density (or acceleration) term is naturally determined in the calculation process. In other words, Navier-Stokes equation can be expressed as:

$$\frac{\mathbf{u}^{n+1} - \mathbf{u}^n}{\Delta t} = \mathbf{RHS}^n + \mathbf{F}^n \quad (2)$$

where $\mathbf{RHS}^n$ includes convective, viscous and pressure terms. If the desired velocity at next timestep is given, then Eq.(2) becomes:

$$\frac{\mathbf{U}^d - \mathbf{u}^n}{\Delta t} = \mathbf{RHS}^n + \mathbf{F}^n . \quad (3)$$

Eq.(3) can be rewritten in terms of the next timestep velocity without being forced, $\mathbf{u}^{noF}$ (which is originally calculated regardless of existence of the forcing term), as

$$\mathbf{U}^d = \mathbf{u}^{noF} + \mathbf{F}^n \Delta t \quad (4)$$

with

$$\mathbf{u}^{noF} = \mathbf{u}^n + \mathbf{RHS}^n \Delta t . \quad (5)$$

From Eqs. (3) and (5), the force density (or acceleration) term can be directly expressed as:

$$\mathbf{F}^n = \frac{\mathbf{U}^d - \mathbf{u}^{noF}}{\Delta t} . \quad (6)$$

For the evaluation of boundary force density term for complex geometries, we have to adopt an interpolation scheme because the boundary, in general, does not match computational nodes. The interpolation schemes can be classified into diffuse and sharp interface schemes. The former usually uses the discrete delta function to evaluate the boundary force on the prescribed boundary points, while the latter uses interpolation from neighboring fluid nodes to evaluate the boundary force on the computational node either inside or outside closest to the boundary. In the diffuse scheme, the boundary force density terms evaluated on the boundary points should also be distributed onto neighboring computational nodes using the discrete delta functions so that the boundary effect may exert on computational process.

On the other hand, the IBM can be coupled with the lattice Boltzmann equation (LBE), which is often called the immersed boundary-lattice Boltzmann method (IB-LBM), instead of Navier-Stokes equations (NSE), because the lattice Boltzmann method (LBM) is also based on the structured non-body-conformal grids and is easy to implement and efficient especially in the parallel computation. Furthermore, the split-forcing concept based on kinetic nature of the LBE allows the simple and direct implementation of the direct-forcing IBM (Kang and Hassan, 2010).

Under the direct-forcing IB-LBM based on split-forcing LBE, several interface schemes have been applied. Kang and Hassan (2008) considered explicit diffuse interface scheme for stationary and moving boundary problems. Wu and Shu (2009) applied implicit diffuse interface scheme to stationary and moving boundary problems. Also, Kang and Hassan (2010) investigated various interface schemes (exterior sharp, explicit diffuse and multi-direct forcing implicit diffuse interface schemes) for stationary boundary problems. The results from Kang and Hassan (2010) revealed that the sharp interface scheme produces more accurate results than the diffuse interface schemes for complex, stationary boundary problems. However, no direct comparison between sharp and diffuse interface schemes for a moving boundary problem was not performed.

Thus, in this paper, we try to compare both sharp and diffuse interface schemes simultaneously for a moving boundary problem under the direct forcing IB-LBM base on the split-forcing LBE and to understand advantages and disadvantages of each scheme. We considered the problem of flow induced by the inline-oscillation of a circular cylinder with Re=100 and KC=5 since both experimental and body-conformal grid method results are available in this case.

NUMERICAL METHODS

Lattice Boltzmann Method

The split-forcing lattice Boltzmann equation (LBE) with an unsteady, non-uniform body force term can be expressed as (Guo et al., 2002):

$$f_\alpha(\mathbf{x} + \mathbf{e}_\alpha \Delta t, t + \Delta t) = f_\alpha(\mathbf{x}, t) - \frac{1}{\tau}\left[f_\alpha(\mathbf{x}, t) - f_\alpha^{(eq)}(\mathbf{x}, t) \right] + F_\alpha \Delta t \quad (7)$$

where $f_\alpha(\mathbf{x},t)$ is the density distribution function for the discrete velocity $\mathbf{e}_\alpha$ in the α-th direction at position $\mathbf{x}$ and time t and τ is dimensionless relaxation time. The equilibrium distribution function $f_\alpha^{(eq)}$ is given as

$$f_\alpha^{(eq)} = w_\alpha \rho \left[1 + \frac{3}{c^2}(\mathbf{e}_\alpha \cdot \mathbf{u}) + \frac{9}{2c^4}(\mathbf{e}_\alpha \cdot \mathbf{u})^2 - \frac{3}{2c^2}\mathbf{u}^2 \right] \quad (8)$$

where the lattice speed c=Δx/Δt and Δx and Δt are the grid size and the timestep size, respectively, and weighting coefficient w_α depends on the discrete velocity set $\{\mathbf{e}_\alpha\}$. The discrete forcing term $F_\alpha(x,t)$ is expressed as (Guo et al., 2002):

$$F_\alpha = \left(1 - \frac{1}{2\tau}\right) w_\alpha \left[3\frac{\mathbf{e}_\alpha - \mathbf{u}}{c^2} + 9\frac{\mathbf{e}_\alpha \cdot \mathbf{u}}{c^4}\mathbf{e}_\alpha \right] \cdot \mathbf{F} . \quad (9)$$

where fluid velocity **u** is determined by

$$\rho \mathbf{u} = \rho \mathbf{u}^{noF} + \tfrac{1}{2}\mathbf{F}\Delta t \quad (10)$$

with

$$\rho \mathbf{u}^{noF} = \sum_\alpha \mathbf{e}_\alpha f_\alpha \quad (11)$$

where $\mathbf{u}^{noF}$ indicates the unforced velocity at the next time step.

Using the Chapman-Enskog multi-scale analysis, we can show that the LBE recovers the Navier-Stokes equation with second-order accuracy.

Immersed boundary-lattice Boltzmann Method

Based on the split-forcing LBE given above, we can derive the following direct-forcing formula (Kang and Hassan, 2010):

$$\mathbf{F}(\mathbf{x}, t+\Delta t) = 2\rho(\mathbf{x}, t+\Delta t)\frac{\mathbf{U}^d - \mathbf{u}^{noF}(\mathbf{x}, t+\Delta t)}{\Delta t} \quad (12)$$

where $\mathbf{U}^d$ is the desired velocity for satisfying the no-slip condition at the next time step and $\mathbf{u}^{noF}$ is the velocity at the next time step without forcing, which can be evaluated using Eq.(11).

Interface Schemes

The IBM requires interface schemes additionally because the boundary, in general, does not match the computational nodes. The interface scheme can be subdivided into diffuse and sharp interfaces schemes. In the sharp interface scheme forcing points are placed on computational nodes closest to the boundary (forcing nodes), while in the diffuse interface scheme, forcing points, on which the boundary force is evaluated, are located on the boundary.

In the sharp interface scheme, to evaluate the boundary force using Eq.(12), $\mathbf{U}^d$ on forcing nodes should be determined so that the closest, corresponding boundary point satisfies the no-slip condition, while $\mathbf{u}^{noF}$ is naturally calculated in the LBM calculation process by using Eq.(11). For the evaluation of $\mathbf{U}^d$, interpolation procedures should be involved. In this study, we consider the exterior sharp interface schemes (Kim et al., 2001) where forcing nodes are located inside solid and closest to the boundary and to evaluate the $\mathbf{U}^d$ linear and bilinear interpolations are used.

In contrast, for diffuse interface schemes, Eq.(12) can be rewritten as:

$$\mathbf{F}(\mathbf{x}_b, t+\Delta t) = 2\rho(\mathbf{x}_b, t+\Delta t)\frac{\mathbf{U}^d - \mathbf{u}^{noF}(\mathbf{x}_b, t+\Delta t)}{\Delta t} \quad (13)$$

where $\mathbf{x}_b$ is the forcing point distributed on the boundary. Here, $\mathbf{U}^d$ can be easily evaluated because the velocity on the boundary is prescribed in general whereas $\mathbf{u}^{noF}$ on the boundary should be evaluated from $\mathbf{u}^{noF}$'s on neighboring computational nodes by interpolation. Furthermore, since the resulting boundary force evaluated is on the boundary, the effects (distributions) on neighboring computational nodes should also be considered. For the interpolation and the force distribution, discrete delta functions can be used in general. In this study, we consider the 4-point discrete delta function, which is defined by (Peskin, 2002):

$$D(\mathbf{x} - \mathbf{x}_b) = \frac{1}{h^2} d_h\left(\frac{x - x_b}{\Delta x}\right) d_h\left(\frac{y - y_b}{\Delta x}\right) \quad (14a)$$

with

$$d_h(r) = \begin{cases} \frac{1}{8}\left(3 - 2|r| + \sqrt{1 + 4|r| - 4r^2}\right), & 0 \le |r| < 1 \\ \frac{1}{8}\left(5 - 2|r| + \sqrt{-7 + 12|r| - 4r^2}\right), & 1 \le |r| < 2 \\ 0, & |r| \ge 2 \end{cases} \quad (14b)$$

We consider the 'implicit' multi-direct-forcing method (Luo et al., 2007; Wang et al., 2008) instead of explicit methods in this study. In the diffuse direct-forcing procedure, velocities on computational nodes (used to evaluate the $\mathbf{U}^d$ on the boundary point and thus the boundary force) are also influenced (updated or forced) by the boundary force. Hence, $\mathbf{U}^d$ obtained from the interpolation using the updated velocities may not satisfy the no-slip condition. Thus, an iterative process is required until such $\mathbf{U}^d$ differences become very small. It should be pointed out that the number of direct-forcing (iterations) (NF) required is known to be relatively small (Kang and Hassan, 2010). In this study, NF=10 is used.

These two schemes based on split-forcing LBE were validated for flows past a stationary circular cylinder in Kang and Hassan (2010).

Surface Force Evaluation

In the IBM, the surface force can be easily evaluated. As depicted in Figure 1, we can consider two control surfaces (S_s and S_f), which can vary with time, and the resulting control volumes surrounded by the two control surfaces (V, V_s, and V_f) in the fluid field.

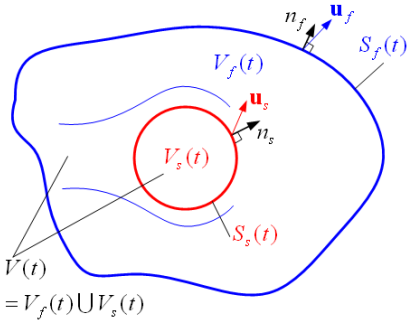

Figure 1 Two time-varying control surfaces (S_s and S_f) and corresponding control volumes (V, V_s, and V_f) in fluid domain.

For the control surface S_s, the force from fluid outside the surface (V_f) to the surface (S_s) can be expressed as:

$$\mathbf{F}_{f\to s} = -\int_{S_s} [\rho\mathbf{u}(\mathbf{u}-\mathbf{u}_s)] + \boldsymbol{\sigma}]\cdot\mathbf{n}_s dS \qquad (15)$$

where $\mathbf{u}_s$ is a boundary velocity of the control surface S_s, $\boldsymbol{\sigma}$ is the viscous stress tensor, and $\mathbf{n}_s$ is its outward surface vector. If the S_s is an impermeable surface, i.e. no flow passes through the surface, then $\mathbf{u} = \mathbf{u}_s$, so that Eq.(15) becomes

$$\mathbf{F}_{f\to s} = -\int_{S_s} \boldsymbol{\sigma}\cdot\mathbf{n}_s dS\,. \qquad (16)$$

For the control volume V_f surrounded by the control surfaces S_s and S_f, from the Cauchy's stress principle, the linear momentum balance can be written as:

$$\frac{\partial}{\partial t}\int_{V_f} \rho\mathbf{u}\, dV = -\int_{S_f} [\rho\mathbf{u}(\mathbf{u}-\mathbf{u}_f)+\boldsymbol{\sigma}]\cdot\mathbf{n}_f\, dS - \int_{S_s} [\rho\mathbf{u}(\mathbf{u}-\mathbf{u}_s)+\boldsymbol{\sigma}]\cdot(-\mathbf{n}_s)\, dS \qquad (17)$$

where $\mathbf{n}_f$ is the outward surface vector of S_f. Using Eq.(16), we can rewritten Eq.(17) as:

$$\frac{\partial}{\partial t}\int_{V_f} \rho\mathbf{u}\, dV = -\mathbf{F}_{f\to s} - \int_{S_f} [\rho\mathbf{u}(\mathbf{u}-\mathbf{u}_f)+\boldsymbol{\sigma}]\cdot\mathbf{n}_f\, dS\,. \qquad (18)$$

For the control volume V covering both V_f and V_s, when boundary forces exist, the linear momentum balance can be expressed as:

$$\frac{\partial}{\partial t}\int_{V_f\cup V_s} \rho\mathbf{u}\, dV = -\int_{S_f} [\rho\mathbf{u}(\mathbf{u}-\mathbf{u}_f)+\boldsymbol{\sigma}]\cdot\mathbf{n}_f\, dS + \int_{V_f\cup V_s} \mathbf{F}\, dV \qquad (19)$$

Subtracting Eq.(18) from Eq. (19), we can obtain the following surface force formula:

$$\mathbf{F}_{f\to s} = \frac{\partial}{\partial t}\int_{V_s} \rho\mathbf{u}\, dV - \int_{V_f\cup V_s} \mathbf{F} dV \qquad (20)$$

where the first term in the left-hand side indicates the added mass effect. If the volume V_s is a rigid solid body with a center-of-mass velocity of $\mathbf{U}_c$, the first term in Eq.(20) can be replaced by $\rho V_s \partial\mathbf{U}_c/\partial t$ (Uhlmann, 2005; Feng and Michaelides, 2008; Liao et al., 2010) and thus Eq.(20) becomes

$$\mathbf{F}_{f\to s} = \rho V_s \frac{\partial\mathbf{U}_c}{\partial t} - \int_{V_f\cup V_s} \mathbf{F} dV\,, \qquad (21)$$

which will be used for the surface force evaluation of the oscillating cylinder in this paper. For reference, if the rigid solid body is fixed or moving with a constant velocity, Eq.(21) simply becomes

$$\mathbf{F}_{f\to s} = -\int_{V_f\cup V_s} \mathbf{F}\, dV\,. \qquad (22)$$

From Eqs. (20), (21), and (22), we can find that if the immersed boundary force is exact, the surface force on solid body can be directly calculated by integrating (or summing in a discrete sense) the boundary force terms regardless of the positions (inside or outside the boundary). This is one of advantages of use of the IBM. Specifically, for sharp interface schemes, since dV directly matches with cell volume (surface in 2D),

$$\int_{V_f\cup V_s} \mathbf{F}\, dV \approx \sum_{i,j} \mathbf{F}_{i,j}\Delta x^2\,. \qquad (23)$$

In contrast, for diffuse interface schemes, the term can be calculated by

$$\int_{V_f\cup V_s} \mathbf{F}\, dV \approx \sum_{b} \mathbf{F}_b \Delta S_b\, \Delta x \qquad (24)$$

where ΔS_b is the arc length of the surface boundary at a forcing point b.

PROBLEM DESCRIPTION

In this study, we investigate the flow induced by an inline-oscillating cylinder in the fluid initially at rest as depicted in Figure 2. The inline-oscillation of the cylinder is governed by the following harmonic oscillation

$$X_c = -A\sin(2\pi f t) \qquad (25)$$

where X_c is the position of the cylinder center and A and f are the amplitude and the frequency of the oscillation, respectively. This flow is characterized by Reynolds (Re) and Keulegan-Carpenter (KC) numbers, which are defined as:

$$\mathrm{Re} = \frac{U_{c,\max} D}{\nu} \quad \text{and} \qquad (26)$$

$$\mathrm{KC} = \frac{U_{c,\max}}{f\, D} \qquad (27)$$

respectively. Here, $U_{c,\max}$ is the maximum velocity of the cylinder during oscillation, D is the cylinder diameter, and ν is kinematic viscosity. In this study, the computation is implemented at Re=100 and KC=5 at which the experimental (LDV) and numerical (body-fitted method) data by Dütsch et al. (1998) are available. Hence, we can quantitatively compare sharp and diffuse interface schemes with them in this problem.

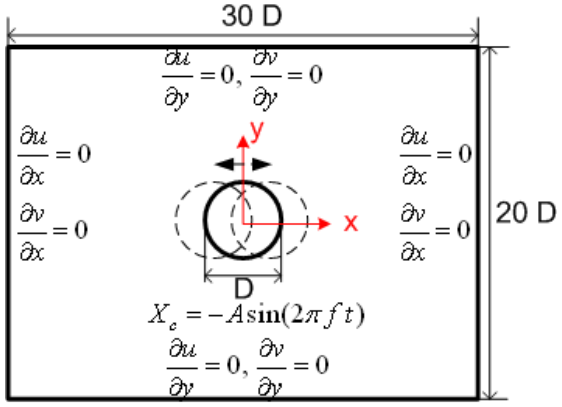

Figure 2 Geometry, computational domain, coordinates, and boundary conditions of the problem.

COMPUTATIONAL CONDITIONS

The computational domain size is 30D×20D (which results from the grid sensitivity study discussed below) and Neumann boundary conditions are imposed on four outer sides of the domain as shown in Figure 2. For the cylinder surface boundary treatments, the IBM with sharp and implicit diffuse interface

schemes are used. In the implicit diffuse interface scheme, forcing points are uniformly distributed on the cylinder boundary with spacing of $\Delta S=\Delta x/1.5$, which is small enough to enable us to obtain size-independent solutions (Kang and Hassna, 2010).

Before comparing the vorticity fields, velocities, and the streamwise force coefficients between interface schemes, we performed the sensitivity study on sizes of computational domain, timestep, and grid. The implicit diffuse interface schemes were used for the sensitivity study. As a target variable, we considered the streamwise force coefficient, which is defined as:

$$C_x = \frac{F_x}{\frac{1}{2}\rho U_{c,\max}^2 D} \tag{28}$$

where F_x is the streamwise surface force and directly obtained from the immersed boundary method using Eq.(21) with Eqs.(23) or (24) depending on the interface schemes.

First, we investigated the effect of domain size by considering three domains of 20D×20D, 30D×20D, and 40D×30D. Figure 3 presents variations of the streamwise force coefficients under the grid of $\Delta x=D/20$ and timestep of $\Delta t=T/1500$ where T is a period of the oscillation. Three results showed very good agreements, so that the domain size of 30D×20D is large enough not to affect the results.

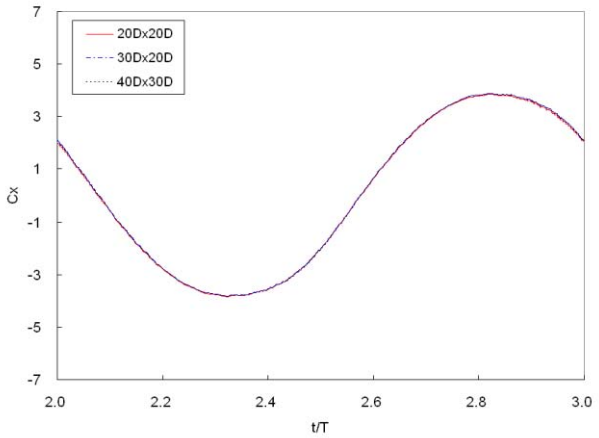

Figure 3 The effect of computational domain size on the streamwise force coefficient.

Next, for the sensitivity of timestep size, in the domain of 30D×20D with D=40Δx, we considered Δt=T/2000, T/3000, and T/4000. Figure 4 shows the resulting streamwise force coefficients. At Δt=T/2000, it shows a slight discrepancy, but at Δt=T/3000 and T/4000, they have almost similar results. Thus, we take Δt=T/3000 in the later calculations.

For the sensitivity of the grid size, we considered D=20, 30, 40, 50, and 60Δx. Figure 5 presents the resulting streamwise force coefficients. It is observed that almost converged results are reached from D=40Δx.

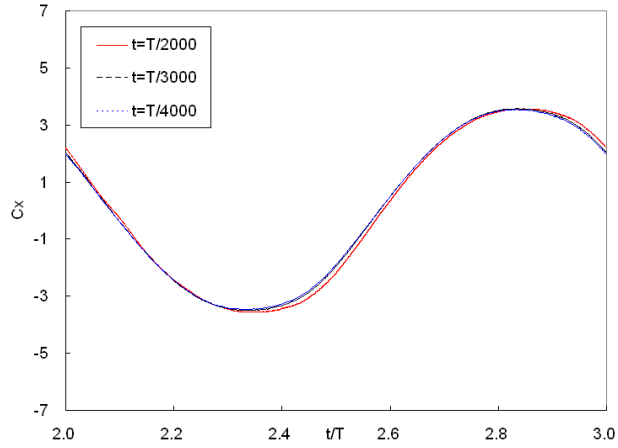

Figure 4 The Effect of timestep size on the streamwise force coefficient.

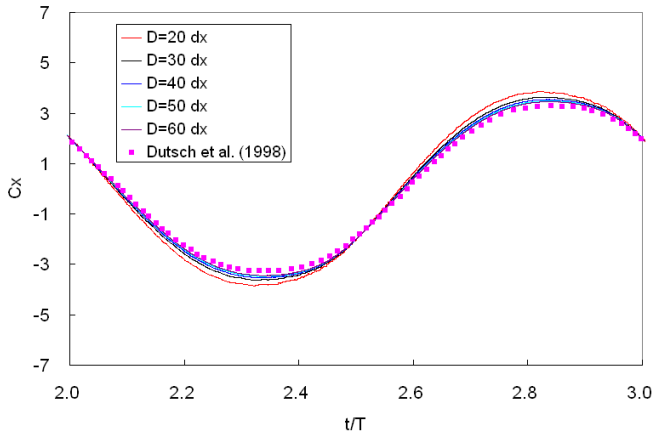

Figure 5 The effect of grid size on the streamwise force coefficient.

RESULTS AND DISCUSSIONS

Figure 6 presents the vorticity fields at four phase angles of 0, 96, 192, and 288°. Both sharp and implicit diffuse interface schemes show qualitatively similar vorticity fields observed by body-fitted grid methods in Dütsch et al. (1998). However, the pressure field (not given here) from the sharp interface scheme haves some wiggles, which may be due to the spurious oscillation. This oscillation is more clearly shown in the variation of streamwise force coefficients in Figure 9(a).

Next, to quantitatively assess two schemes, we compare the velocity data at locations of x = -0.6, 0, 0.6, and 1.2D in phase angles of 180, 210, and 330° because Dütsch et al. (1998)'s data are available for these cases. Figures 7 and 8 present the horizontal and the vertical velocities at a phase angle of 330° obtained from the sharp interface scheme and the implicit diffuse interface scheme, respectively. Both figures include experimental and numerical data of Dütsch et al. (1998). We can observe that both schemes have good agreements with Dütsch et al.'s results. In other phases (180 and 210°), in spite

of not being presented in this paper, good agreements between both schemes and Dütsch et al. are observed.

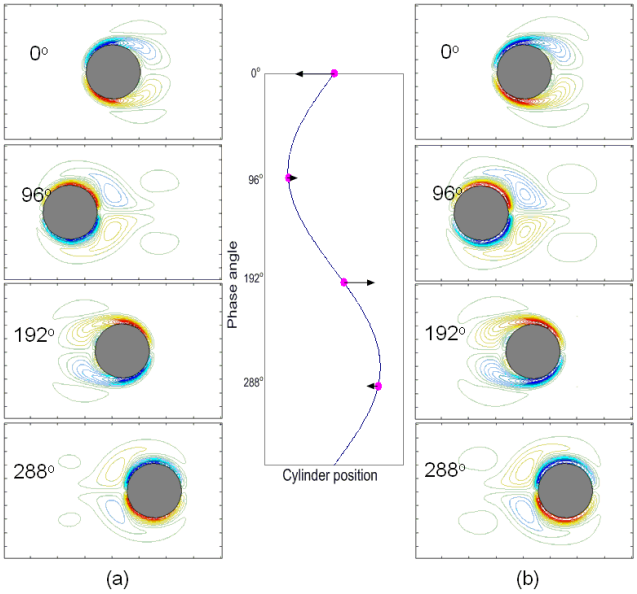

Figure 6 Vorticity fields obtained from (a) the sharp interface scheme and (b) the implicit diffuse interface scheme.

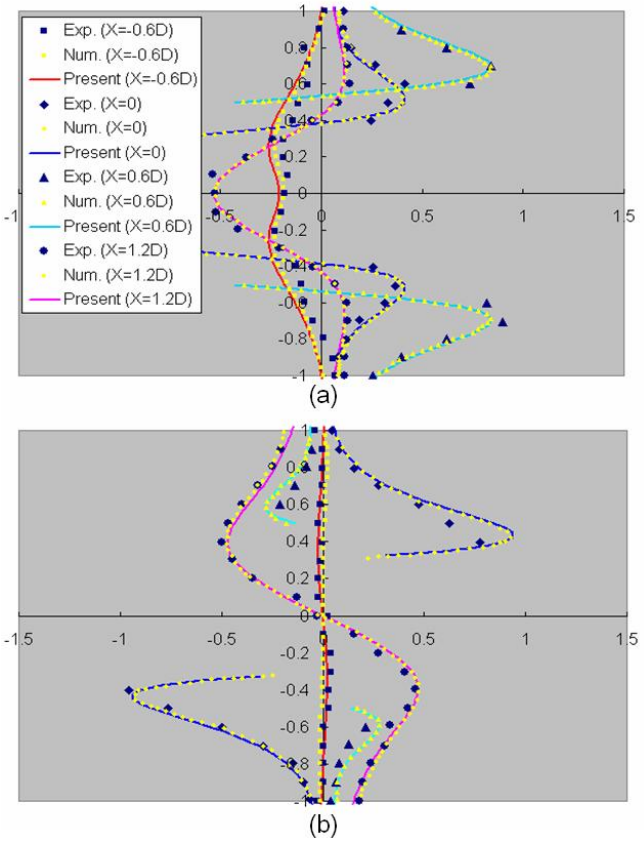

Figure 7 Comparison of (a) horizontal and (b) vertical velocities at a phase angle of 330^o at x = -0.6, 0, 0.6, and 1.2D between the sharp interface scheme and Dütsch et al. (1998).

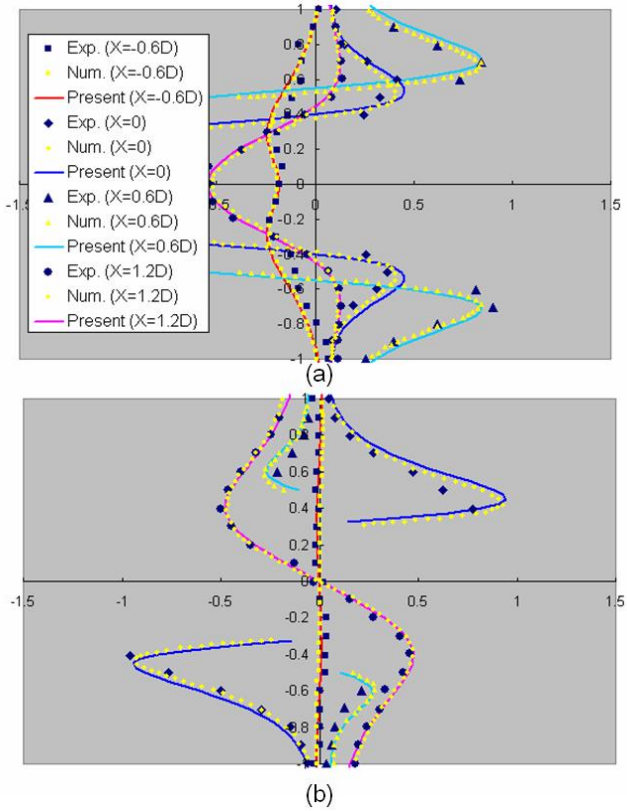

Figure 8 Comparison of (a) horizontal and (b) vertical velocities at a phase angle of 330^o at x = -0.6, 0, 0.6, and 1.2D between the implicit diffuse interface scheme and Dütsch et al. (1998).

Figure 9 presents the streamwise force coefficient variation obtained from the exterior sharp interface scheme with D=40Δx. As mentioned above, it shows spurious oscillations due to discontinuous change of nodes used in the interpolation as shown in Figure 9(a). However, if we adopt the filtering (for example, low pass FFT filtering) or smoothing as Miller and Peskin (2004) and Shen et al. (2009) recommended, it shows the good agreement with Dütsch et al. (1998)'s data as presented in Figure 9(b). It should be pointed out that we also tested sharp interface schemes which had been developed for reducing such spurious oscillations by Yang and Balaras (2006) and Liao et al. (2010), but only minor improvements were obtained under the IB-LBM based on split-forcing LBE. This may be due to the difference between the Navier-Stokes equations and the lattice Boltzmann equations.

According to the grid sensitivity study using other resolutions (D=20, 30, 40, 50, and 60Δx), despite not being given here, the results almost converges from D=30Δx. In contrast, as presented in Figure 5, when adopting the diffuse interface schemes, the streamwise force coefficients show bigger discrepancy. Especially, the largest discrepancies occurred near phase angles of 90 and 270^o (where the magnitude of acceleration is the maximum) and the least discrepancies occurred at angle phases of 0 and 180^o (where the magnitude of acceleration is zero). In other words, the larger

magnitude of acceleration the cylinder has, the larger discrepancy the surface force coefficient has. It should also be noted that to the authors' knowledge, no direct-forcing IBM with diffuse interface schemes except Wang et al. (2009) was documented for this problem. In Wang et al. (2009), the multi-direct-forcing IBM with a diffuse interface scheme was used but the governing equations were based on vorticity equations, not pressure equations. In their calculation results of the force coefficient, for the comparison, they also provided those from the direct-forcing IBM with diffuse interface schemes based on the pressure equation, which showed large discrepancies near phase angles of 90 and 270^o as in this study. On the other hand, from the results of flow past a stationary circular cylinder in Kang and Hassan (2008), we can observe that the diffuse interface schemes can have the maximum 5% larger drag coefficients than body-fitted methods at D=40Δx. However, the largest discrepancy for the moving cylinder in this study is about 8.0% under D=40Δx.

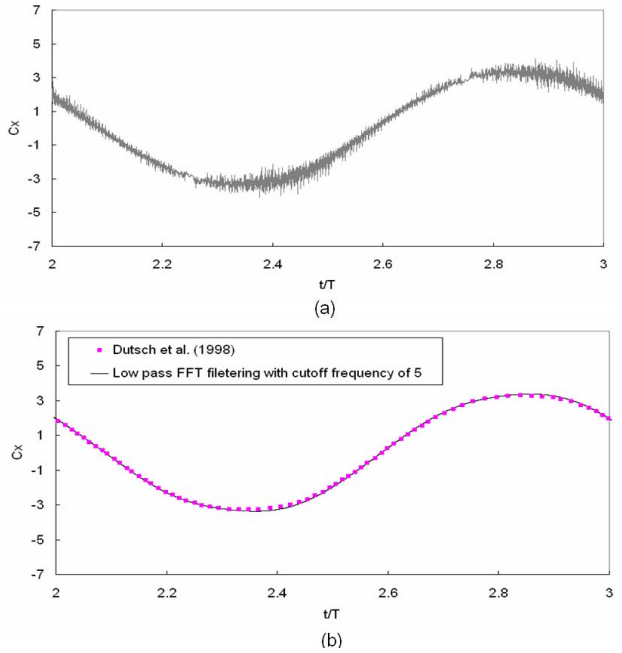

Figure 9 Streamwise force coefficients (a) before and (b) after low pass FFT filtering.

In order to mitigate the over-prediction, we can adopt the concept of the effective radius (Höfler and Schwarzer, 2000), which corrects over-estimation of the drag coefficient due to the effect of diffuse boundary. From the stationary results in Kang and Hassan (2010), we can approximate the effective radius (r_{eff}) as

$$r_{eff} \approx r_s + 0.5\Delta x. \qquad (29)$$

Thus, we retract the surface on which the forcing points are distributed by an amount of 0.5Δx from the geometric surface. The resulting surface coefficient variation at D=40Δx is given in Figure 10, which shows a good agreement with Dütsch et al. (1998)'s data. Here, the corrected radius of 19.5Δx was used for the distribution of forcing points. It should be noted that the radius for the evaluation of V_s in the added mass term (the first term in RHS of Eq.(21)) is the geometric radius (r_s), not the corrected radius.

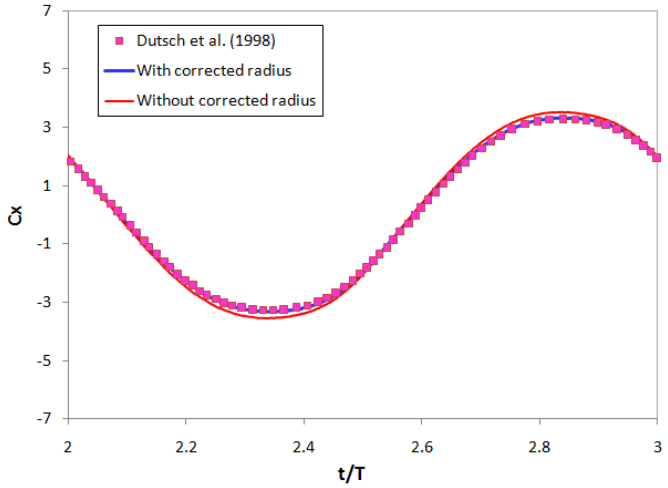

Figure 10 The streamwise force coefficients with and without considering the diffuse boundary effect.

CONCLUSIONS

In this study, we investigated the effects of interface schemes on results of the moving boundary problem. The evaluation method of the boundary force was the direct-forcing method based on the split-forcing lattice Boltzmann equations (Kang and Hassan, 2008, 2010), i.e. direct-forcing IB-LBM. The interface schemes considered were the exterior sharp interface scheme (Kim et al., 2001) and the implicit diffuse scheme (Luo et al., 2007). For the test problem, the flow induced by an inline-oscillating cylinder at quiescent fluid with Re=100 and KC=5 was considered because the test case has both the experimental data measured by LDV and the numerical results based on the body-fitted methods by Dütsch et al. (1998).

Velocity results (vorticity, horizontal and vertical velocities) from both schemes showed overall good agreements with experimental and body-fitted calculation data of Dütsch et al. (1998). However, the sharp interface scheme showed spurious oscillations in the streamwise surface force coefficient, although after filtering or smoothing it showed good agreement with experiment. However, it still showed wiggles in pressure field.

In contrast, the diffuse interface scheme produced smooth variations in the surface force coefficient and the pressure fields due to the use of discrete delta function, which involves the information of interior nodes inside the solid boundary, thus smoothing the discontinuous change of nodes. However, such a property of the discrete delta function reduced the accuracy. Especially, the reduction of accuracy was larger in the oscillating cylinder in this study than in the fixed cylinder

(Kang and Hassan, 2010). This discrepancy could be mitigated or removed by the considering the effective radius.

Thus, it is expected that that the diffuse interface scheme with the corrected radius for the forcing point distribution can be effectively applied to fluid-surface interaction problems, such as fluid-induced vibration, and moving particle problems.

REFERENCES

DÜTSCH, H., DURST, F., BECKER, S., LIENHART, H., Low-Reynolds-number flow around an oscillating circular cylinder at low Keulegan-Carpenter numbers, *J. Fluid Mech.*, Vol. 360, 1998, pp. 249-271.

FENG, Z.G., MICHAELIDES, E.E., Robust treatment of no-slip boundary condition and velocity updating for the lattice-Boltzmann simulation of particulate flows, *Comput. Fluids*, Vol. 38, 2009, pp. 370-381.

GLOWINSKI, R., PAN, T.-W., HESLA, T.I., JOSEPH, D.D., A distributed Lagrange multiplier / fictitious domain method for particulate flows, *Int. J. Multiphas. Flow*, Vol. 25, 1999, pp. 755-794.

GLOWINSKI, R., PAN, T.-W., HESLA, T.I., JOSEPH, D.D., PERIAUX, J., A fictitious domain approach to the direct numerical simulation of incompressible viscous flow past moving rigid bodies: Application to particulate flow, *J. Comput. Phys.*, Vol. 169, 2001, pp. 363-426.

GOLDSTEIN, D., HANDLER, R., SIROVICH, L., Modeling a no-slip boundary with an external force field, *J. Comput. Phys.*, Vol. 105, 1993, pp. 354-366.

GUO, Z., ZHENG, C., SHI, B., Discrete lattice effects on the forcing term in the lattice Boltzmann method, *Phys. Rev. E*, Vol. 65, 2002, pp. 046308.

HÖFLER, M., SCHWARZER, S., Navier-Stokes simulationn with constraint forces: Finite-difference method for particle-laden flows and complex geometries, *Phys. Rev. E*, Vol. 61, 2000, pp. 7146-7160.

HU, H.H., PATANKAR, N.A., ZHU, M.Y., Direct numerical simulations of fluid-solid systems using arbitrary Lagrangian-Eulerian technique, *J. Comput. Phys.*, Vol. 169, 2001, pp. 427-462.

KANG, S.K., HASSAN, Y.A., An immersed boundary-lattice Boltzmann method for large particle sedimentation. *The 7th International Topical Meeting on Nuclear Reactor Thermal Hydraulics, Operations and Safety (Nuthos7)*, Seoul, Korea, 2008.

KANG, S.K., HASSAN, Y.A., A comparative study of direct-forcing immersed boundary-lattice Boltzmann methods for stationary complex boundaries, *Int. J. Numer. Meth. Fluids*, 2010, DOI: 10.1002/fld.2304.

KIM, J., KIM, D., CHOI, H., An immersed-boundary finite-volume method for simulations of flow in complex geometries. *J. Comput. Phys.*, Vol. 171, 2001, pp. 132-150.

LIAO, C.C., CHANG, Y.W., LIN, C.A., MCDONOUGH, J.M., Simulating flows with moving rigid boundary using immersed boundary method, Comput. Fluids, Vol. 39, 2010, pp. 152-167.

LUO, K., WANG, J., CEN, K., Full-scale solutions to particle-laden flows: multidirect forcing and immersed boundary method. *Phys. Rev. E*, Vol. 76, 2007, pp 066709.

MILLER, L.A., PESKIN, C.S., When vortices stick: an aerodynamic transition in tiny insect flight. *J. Exp. Biol.*, Vol. 207, 2004, pp. 3073-3088.

PESKIN, C.S., Flow patterns around heart valves: a numerical method, *J. Comput. Phys.*, Vol. 10, 1972, pp. 252-271.

PESKIN, C.S., Immersed boundary method. *Acta Numerica*, Vol. 11, 2002, pp. 479-517.

SHEN, L., CHAN, E.-S., LIN, P., Calculation of hydrodynamic forces acting on a submerged moving object using immersed boundary method, *Comput. Fluids*, Vol. 38, 2009, pp. 691-702.

UHLMANN, M., An immersed boundary method with direct forcing for the simulation of particulate flows, *J. Comput. Phys.*, Vol. 209, 2005, pp. 448-476.

WANG, Z., FAN, J., LUO, K., Combined multi-direct forcing and immersed boundary method for simulating flows with moving particles. *Int. J. Multiphase Flow*, Vol. 34, 2008, pp. 283-302.

WANG, Z.L., FAN, J.R., CEN, K.F., Immersed Boundary method for the simulation of 2D viscous flow based on vorticity-velocity formulation, *J. Comput. Phys.*, Vol. 228, 2009, pp. 1504-1520.

WU, J., SHU, C., Implicit velocity correction-based immersed boundary-lattice Boltzmann method and its applications. *J. Comput. Phys.*, Vol. 228, 2009, pp. 1963-1979.

YANG, J., BALARAS, E., .An embedded boundary formulation for large-eddy simulation of turbulent flows with moving boundaries, *J. Comput. Phys.*, Vol. 215, 2006, pp. 12-40.